Contents lists available at ScienceDirect

Polymer

journal homepage: http://ees.elsevier.com

Effects of organo-LDH dispersion on thermal stability, crystallinity and mechanical features of PLA

Nicolas Delpouve [a], Allisson Saiter-Fourcin [a], Serena Coiai [b], Francesca Cicogna [b], Roberto Spiniello [b], Werner Oberhauser [c], Stefano Legnaioli [b], Randa Ishak [d], Elisa Passaglia [b,*]

[a] Normandie Univ, UNIROUEN Normandie, INSA Rouen, CNRS, Groupe de Physique des Matériaux, 76000, Rouen, France
[b] Italian National Council for Research - Institute for the Chemistry of OrganoMetallic Compounds (CNR-ICCOM) SS Pisa, Via Moruzzi 1, 56124, Pisa, Italy
[c] Italian National Council for Research - Institute for the Chemistry of OrganoMetallic Compounds (CNR-ICCOM), Via Madonna Del Piano 10, 50019, Sesto Fiorentino, Firenze, Italy
[d] Department of Civil and Industrial Engineering, University of Pisa, Largo L. Lazzarino 1, 56122, Pisa, Italy

ARTICLE INFO

Keywords
PLA nanocomposites
Morphology
Thermal and mechanical properties
Crystallinity

ABSTRACT

PLA-based composites were prepared by mixing the polymer in the melt with organophilic Mg/Al LDH and Mg Stearate. The obtained materials were therefore characterized in comparison with the unfilled PLA with the aim of investigating the relationships between the morphology of the polymer composites and their thermal stability, crystallinity and mechanical properties. The degradative effects induced by the presence of O-LDH and its organic component (*i.e* alkyl carboxylates used as surfactant) were evaluated by analysing the samples with SEC and TGA under standard and modulated conditions, in the presence of nitrogen and air. The collected results proved that the main effects on degradation are due to inorganic reactive species and to increased interfacial surface owing to intercalated/exfoliated morphology. The main thermal transitions of the composites were studied by XRD and DSC (even in modulated conditions) before and after annealing processes at different temperatures. The results inherent to the percentage of crystallinity, the content of rigid amorphous fraction (RAF), and the main size of crystalline domains were discussed by considering the filler nature/content, its dispersion degree in polymer matrix and the annealing temperature. By crystallization at 80 °C the filler promoted both RAF and crystallites size. Unlike unfilled PLA, the composites showed an increase of the stiffness and a general loss of ductility which were tentatively ascribed to annealing at 80 °C and to the extent of interfacial interactions.

1. Introduction

PLA-based nanocomposites prepared by dispersing 2D nanostructured systems into the polymer matrix have attracted considerable attention due to the possibility of obtaining materials with increased mechanical and barrier properties [1]. In particular, thanks to the large extent of polymer-inorganic interface, layered nanofillers can act as nucleating agents and their dispersion can help tailoring the microstructure of PLA, which is reported to play a significant role in barrier properties and then it can be considered a key parameter in designing materials for packaging applications [2,3].

Being PLA a biodegradable and food contact allowed polymer that derived from renewable resources, the nanometric dispersion of 2D systems, such as layered double hydroxides (LDHs) or hydrotalcite-like compounds, which can be synthesized as non-toxic and food-contact approved, has received great attention in recent years for preparing PLA-based nanocomposites for food bio-packaging applications. By this way, PLA composites with improved optical and barrier properties as well as with enhanced crystallinity have been successfully obtained [4,5]. In this regard LDHs are a class of synthetic anionic clays with a host–guest nanolayered structure consisting of positively charged metal hydroxide sheets in which guest molecules (generally $-CO_3^{2-}$, and/or $-OH^-$ in native LDH) are accommodated, together with water molecules [6]. The nanometric dispersion of LDHs (*i.e.* delamination into single layers) into apolar polymers (*e.g.* polyolefins and polyesters) is possible only if native LDH is organophilically modified. The organo-modification of LDHs is usually achieved through the use of chemicals suitable for food-packaging applications and acting as surfactants, such as alkyl carboxylates (*e.g.* oleate, stearate and palmitate), which can be used alone or as a mixture [7–12]. Other organic molecules suitable for packaging (*e.g.* alkyl sulphates, antioxidant, dyes) [13–15] and also bearing specific functionalities are described as guest molecules of organo-LDH systems and their dispersion in PLA is widely reported [4,5,17–19].

* Corresponding author.
E-mail address: passaglia@pi.iccom.cnr.it (E. Passaglia)

https://doi.org/10.1016/j.polymer.2020.122952
Received 16 June 2020; Received in revised form 29 July 2020; Accepted 16 August 2020
Available online xxx
0032-3861/

Different methods can be used to produce organo-LDHs including direct synthesis and regeneration [14]. However, a common strategy is the organo-modification by anion exchange from LDH precursors thus producing organic-inorganic hybrid systems (organophilic-LDH, O-LDH), where the percentage of the organic fraction, capable of promoting the intercalation of the PLA chains between the layers of the hydroxides, is generally greater than 40% by weight. Several reports have described the mixing of these hybrid systems with PLA, both in the melt and in solution, to afford nanocomposites with different morphologies and thermo-mechanical properties depending on the organic modifiers, metal cations of the hydroxide layers, composition and dispersion procedures. Indeed, by considering the numerous parameters affecting the ultimate features of such composites, the findings outlined in these reports about morphological, thermal and mechanical properties do not always agree.

The morphology of PLA-based composites with organophilic LDH obtained by using sodium dodecyl sulphate, sodium benzene sulfonate and carboxylates as modifiers looks generally exfoliated when analysed by XRD. Indeed the XRD patterns of these PLA-based composites do not show diffraction signals due to O-LDH even if single layers mixed with a small fraction of nanostacks are generally present. Furthermore, in a few cases, tactoids and large aggregates of several microns and likely due to flocculation have been evidenced by SEM and TEM analyses [4,9,11,12,16,17,20]. A small quantity of hybrid system (between 1 and 3% by weight), induces significant variations of the molecular structure and of the thermal properties of the PLA. A decrease in molecular weight, especially if mixing takes place in the melt, is reported, even if it has not been fully and clearly discussed which of the two components of the hybrid system (the organic or the inorganic fraction, that means the surfactant or the layered double hydroxide) is actually responsible for this behaviour [10–12,16,20]. Similar evidence is discussed as a very general trend with regard to the thermal stability of composites, but not all the results are in agreement. Depending on the metal cations pair that form the hydroxide layers and on the chemical nature of the surfactant, both an increase or a decrease of the thermal stability of the composites have been reported [4,5,12,17,18,21,22]. Composites with Mg/Al-LDH modified with sodium dodecyl sulphate, containing 1–3 wt % of O-LDH, showed a detriment of the thermal stability with respect to PLA matrix [4]. Similar behaviour is described for the composites obtained by dispersing O-LDH modified with carboxylates [10,12] or with carboxylic acid-terminated PLA (PLA-COOH) [9,17]. Other reports have described the use of LDHs modified with sodium dodecylbenzene sulfonate and plasticizers[21]. as well as of LDHs constituted by a different pair of metal cations (Ni/Al, Zn/Al) and modified with complexants [5] or phosphorus compounds [18], evidencing that these hybrid systems are able to increase the thermal stability of PLA once dispersed at nanoscale level.

Furthermore, the stiffness and mechanical strength of PLA are raised by its crystalline fraction obtained by annealing. The crystallinity of PLA in PLA/LDH or PLA/O-LDH composites is generally higher than that of pristine PLA because of the nucleating action exerted by the LDH and O-LDH. Different numerical values depend on the quantity of LDH and on kinds of metal cations of hydroxide layers [5,16,22]. Nevertheless several papers discuss the opposite trend (a decrease of crystallinity) explaining this evidence on the basis of an inhomogeneous distribution of crystallites in proximity of LDH [12,20]. The mechanical features of these composites have been investigated in standard conditions and improvements of the performances are generally reported [4,5,10,21].

To the best of our knowledge, nothing is reported so far concerning the thermal behaviour of PLA in PLA/O-LDH nanocomposites induced by different annealing temperatures, which are able of generating different crystalline phases, and no data have been reported about the effects of this thermal treatment on mechanical features of composites.

In this paper we shed more light on the thermal behaviour of composites obtained by dispersing O-LDH (modified by alkyl carboxylates) in PLA matrix and prepared in the melt. The morphology and the microstructure were characterized by size exclusion chromatography (SEC), X-ray diffraction analysis (XRD), scanning electron microscopy (SEM), Fourier transform infrared spectroscopy (FTIR), and micro-Raman spectroscopy. The thermal stability was investigated by thermogravimetric and modulated-temperature thermogravimetric analyses (TGA and MT-TGA) carried out under nitrogen and oxygen atmosphere and the results were correlated with composites' composition and morphology. Standard differential scanning calorimetry (DSC) and modulated temperature DSC (MT-DSC) as well as XRD analysis were used to investigate the percentage of crystallinity, the size of crystalline domains and the content of rigid amorphous fraction (RAF) as a function of different annealing temperatures. Finally, preliminary mechanical tests are here reported before and after annealing at 80 °C.

2. Experimental part

2.1. Materials

Poly (lactic acid) PLA, 96% L-lactic acid (Natureworks [melt flow index 4–8 g/10 min (2.16 kg, 190 °C)], was used as the polymer matrix. Before processing, PLA was dried in a vacuum oven at 110 °C for 18 h. Poly (butylene succinate adipate) (PBSA) with a melt flow index (MFI) of 1.4 g/10 min (2.16 kg, 190 °C) and $\overline{M_n}$ = 52 000 g/mol, $\overline{M_w}$ = 112 000 g/mol (as determined by size exclusion chromatography, SEC) was used as coupling agent. Layered double hydroxide organically modified with hydrogenated fatty acids (O-LDH) (Perkalite F100, Azko Nobel, modifier content 55 wt%) and magnesium stearate (Mg-Stearate) (Sigma Aldrich, technical grade) were used after drying both at 110 °C for 12 h.

2.2. Composite preparation

Composite samples were prepared by melt blending the PLA matrix with different content of O-LDH (PLA_O-LDH_1 and PLA_O-LDH_2). In addition, for comparison purposes, PBSA was added as coupling agent to test its capability to improve the interfacial interaction between PLA and the nanostructured filler (PLA_O-LDH_1_PBSA). In one sample, MgStearate was added to PLA and it was used to investigate the effect of surfactant employed as LDH modifier onto the ultimate properties of PLA (sample coded as PLA_MgStearate). Finally, a blank experiment consisting of PLA treated in Brabender at 180 °C was prepared (PLA_180). Samples were prepared in a discontinuous mechanical mixer Brabender (PlastographOHG47055, 30 mL chamber) at 180 °C for 10 min and setting a rotor speed of 60 rpm. The amount of polymer introduced was 20 g for all the runs (PLA and eventually PBSA) and the filler was added after 3 min. During the runs the torque values were monitored and the final *Δtorque* values are reported in Table 1 to-

Table 1
Samples composition, *Δtorque* values and $\overline{M_n}$ and $\overline{M_w}$ data (from SEC analysis).

Sample code	O-LDH (wt%)	*Δtorque* [a] (Nm)	$\overline{M_n}$(D)	$\overline{M_w}$(D)
PLA	–	–	125 000	190 000
PLA_180 [b]	0	0.6	102 000	174 000
PLA_O-LDH_1	1	0.0	72 000	135 000
PLA_O-LDH_2	2	3.4	65 000	121 000
PLA_O-LDH_1_PBSA [c]	1	2.7	81 000	148 000
PLA_MgStearate [d]	0	1.9	68 000	139 000

[a] Evaluated as torque at 2min-torque at 10 min.
[b] PLA treated at 180 °C without any additive.
[c] Sample containing 1 wt% of PBSA with respect to PLA.
[d] Sample containing 1 wt% of MgStearate added after 3min.

Table 2
Detailed analysis of crystalline region in neat and filled samples.

Annealing at 80 °C	*FWHM* (Θ)	*D* (nm)	Annealing at 130 °C	*FWHM* (Θ)	*D* (nm)
PLA_180	0.6776	12.9	PLA_180	0.4725	18.6
PLA_O-LDH_1	0.5556	15.8	PLA_O-LDH_1	0.4926	17.8
PLA_O-LDH_2	0.5338	16.4	PLA_O-LDH_2	0.4687	18.8
PLA_MgStearate	0.5451	16.1	PLA_MgStearate	0.4920	17.8
PLA_O-LDH_1_PBSA	0.5563	15.8	PLA_O-LDH_1_PBSA	0.4973	17.7

gether with the sample composition and their molecular weight (see Table 2).

2.3. Composites characterization

Size exclusion chromatography (SEC) analysis of the samples was performed in $CHCl_3$ at a flow rate of 0.3 mL min^{-1} using an Agilent Technologies 1200 Series instrument equipped with a degasser, an isocratic HPLC pump, a refractive index (RI) detector, and two PLgel 5 μm MiniMIX-D columns conditioned at 35 °C. The system was calibrated with polystyrene standards in a range from 500 to 3×10^5 g mol^{-1}. Samples were dissolved in $CHCl_3$ (2 mg mL^{-1}) and twice-filtered through a 0.20 μm syringe filter before analysis. Number average molecular weight ($\overline{M_n}$) and weight average molecular weight ($\overline{M_w}$) were calculated using the Agilent ChemStation software and are compiled in Table 1.

Attenuated Total Reflectance (ATR-FTIR) spectra were recorded at room temperature with a PerkinElmer Two Spectrometer equipped with an ATR accessory with diamond crystal. The spectra were generally acquired between 4000 and 400 cm^{-1} with a resolution of 4 cm^{-1} using 16 scans. The composites were analysed onto films prepared hot-pressing using a press Carver 3851CE: T = 180 °C, 3 bars, 3 min.

The micro-Raman analysis was performed using a Renishaw micro-Raman inVia instrument equipped with a 1800 grooves/mm diffraction grating, a CCD detector, and a 50 × magnifying lens. The instrument has a Nd:YAGlaser source at $\lambda = 532$ nm wavelength. The samples were analysed as polymer films.

Wide-angle X-ray diffraction (WAXD) analysis was performed at room temperature with a X'Pert PRO (PANalytical) powder diffractometer in the 1.5–30.0° 2θ range applying a scan speed of 0.01601° min^{-1}, using a Cu Kα radiation (1.5406 Å). The samples were analysed after annealing at 80 °C and at 130 °C for 8 h in a oven (under vacuum) in order to induce the well-known α′- and α-crystalline phases for PLA respectively. The thickness of crystal lamellae was determined by applying the Scherrer equation. The full width at half maximum (*FWHM*) in radians for the crystallographic (203) plan was calculated by means of the Origin software, using a Gaussian function which gave the best fitting results (i.e. error less than 8%). LaB_6 was used to determine the contribution of the experimental set-up to the line broadening of the 203 reflection.

A first set of standard thermogravimetric analyses (TGA) was performed from 30 up to 900 °C at 10 °C/min in a Netzsch® TG 209 analyser under nitrogen and oxygen at a dynamic gas flow of 30 mL min^{-1}. Al_2O_3 crucible has been used. The sample masses were ranging between 10 and 15 mg. Modulated temperature thermogravimetric analysis (MT-TGA) experiments were then performed in platinum pans compatible with high temperature, from 30 to 700 °C, in a Thermal Analysis® Discovery apparatus. The sample masses were about 5 mg. Each calibration procedure included a baseline, a calibration in temperature and a calibration in mass. The calibration in temperature was done using the Curie point of nickel as reference. The calibration in mass was done using standard masses, and the calibration in mass loss was done using calcium oxalate as reference. MT-TGA experiments were performed under nitrogen and oxygen at a purge rate of 25 mL min^{-1} with a balance purge of nitrogen at 25 mL min^{-1}. The modulation parameters (i.e. amplitude = 5 °C, period = 200 s, and heating rate = 5 °C/min, were chosen to provide a minimum of five cycles within the degradation process range. MT-TGA theory has been described in literature [23–27]. It is an efficient technique to investigate the influence of both chain scission and changes in functionality on the kinetics of decomposition since it allows determining the activation energy E_a (eq .1) of the different processes involved in the degradation of a material from a single experiment.

$$E_a = \frac{R\ \left(T^2 - A^2\right)\ \mathrm{Ln}\left(\frac{d\alpha_p}{d\alpha_v}\right)}{2\ A} \quad (1)$$

Where T is the average value of oscillatory temperature; A is the amplitude of the temperature oscillation; and $d\alpha_p/d\alpha_v$ is the ratio for adjacent peaks and valleys, of the periodic rate of reaction.

The modulated temperature differential scanning calorimetry (MT-DSC) investigations were performed with a Q100 calorimeter (TA instrument®). The instrument was calibrated for heat flow, temperature and baseline using standard Tzero technology. The nitrogen flow was 50 mL min^{-1} for all the experiments. The calibration of the temperature was carried out using indium and zinc as standards, and the calibration in energy was carried out using standard indium. The calibration of the specific heat capacity was carried out using sapphire as a reference. Modulation parameters were defined as follow: 2 °C/min heating rate, 0.318 °C amplitude, and 60 s period. These parameters correspond to heat only conditions which are suitable for simultaneous investigations of glass transition, crystallization and melting. MT-DSC measurements were performed on amorphous samples quenched from the melt, and semi-crystalline samples obtained by isothermal crystallization from the melt at 80 °C and 130 °C for 8 h to favor the formation of α′- and α-crystal polymorphs of PLA, respectively. The cooling of the melt was performed as fast as possible in-situ in order to prevent crystallization before reaching the crystallization temperature. The morphological analysis was performed by using Field Emission - Scanning Electron Microscope, FE-SEM with a FEI Quanta 450 ESEM FEG in SE mode (instrument located at CISUP-University of Pisa).

Stress-strain measurements have been performed by Instron mod. 5966 E2 (5 mm min^{-1}). Films of the samples were prepared by compression-molding at 180 °C and cut to have specimens suitable for the analysis (1 cm × 10 cm). The measurements were performed onto the films as obtained and even onto the films after annealing at 80 °C (under vacuum) for 8 h.

3. Results and discussion

3.1. Structural and morphological analysis

During the runs the torque evolution was monitored and, with the exception of the sample PLA_O-LDH_1, a general drop of the apparent melt viscosity was observed, suggesting a decrease in the molecular weight of PLA (Table 1). SEC results are in agreement with this trend and showed that the addition of both the fillers led to a decrease of PLA molecular weight, particularly by increasing the content of O-LDH, and the effect was only partially restrained by using PBSA as coupling agent. This evidence, already observed for similar PLA composites [11,20], can be attributed to catalytic degradation of PLA induced by Al and Mg ions and in particular by basic Mg–OH sites on the layer surfaces [28]. Besides this effect, traces of water in the intergallery spaces might contribute to degradation due to hydrolytic chain scission [12,16]. Interestingly, it has been evidenced that also stearate salt caused a PLA molecular weight reduction, possibly due to its catalytic role in degradation mechanism, as already reported [29]. This re-

sult indicates that carboxylate chain ends may act as degrading agents [11] even during the mixing, by probably triggering a back-biting mechanism [9,17], even if Mg ions and residual water can determine the same final effect. The carboxylate-modified LDH (O-LDH) was observed, indeed, as more effective in provoking the degradation with respect to unmodified LDH [10]; nevertheless, this result is likely affected by the better dispersion of the O-LDH with respect to that obtained by using an unmodified LDH due to more effective interfacial interactions between hydroxide surface and PLA macromolecules, enlarging the contact area between polymer and filler [9,10].

The XRD spectrum of O-LDH showed an intense (003) reflection at $2\theta = 3.18°$ corresponding to a basal spacing of 2.8 nm in agreement with surfactant content and its arrangement in the interlayer spacing [30]; whereas the composites did not show the characteristic diffraction peaks of O-LDH, suggesting a good dispersion as generally reported for similar compositions (Fig. 1) [9,11,19]. However, the absence of diagnostic diffraction peaks due to O-LDH cannot be considered a proof for complete exfoliation of the nanostructured filler, because the layer structures, which are not in parallel registry, are not detected. Indeed, polymer-lamellae aggregations generating three-dimensional frameworks have been observed for composites designed with the same or similar nanostructured filler [7,19,31]. SEM analysis of sample PLA_O-LDH_1 (Figure ESI 1) and of sample PLA_O-LDH_2 (Fig. 2) clearly evidenced the presence of aggregates; in particular the fractured area of sample PLA_O-LDH_2 showed the presence of regions containing macro-aggregates composed by inorganic lamellae with intercalated polymer fractions which are related to each other with linking zones due to the polymeric chains. Thanks to the organo-modification of LDH, the polymer (specifically PLA or PBSA) is able to intercalate and destroy the piled ordered lamellae, but macro-aggregates can be generated as a result of interactions between functionalities (such as C═O of PLA and –OH of LDH) providing flocculation of disordered hybrid systems (micro and nano-stacks) containing both LDH layers and polymer chains [9].

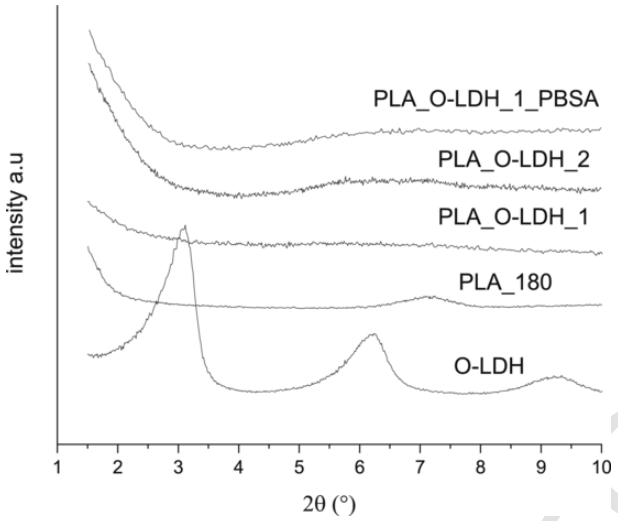

Fig. 1. XRD Patterns of O-LDH, PLA_180 and all the composites containing O-LDH.

The Leica optical microscopy combined with micro-Raman instrument confirmed the presence of inclusions with different size ranging from several microns to sub-microns (Figure ESI 2a shows pictures collected on different portions of films of composites PLA_O-LDH_1 and PLA_O-LDH_2). These inclusions seem to be morphologically organized in disordered stacked structures, as expected and in agreement with SEM results. Differently, the non-ordered microparticles of MgStearate present in the PLA_MgStearate composite show a more globular shape (Figure ESI 2b).

The ATR-FTIR spectrum of O-LDH (Figure ESI 3) showed the diagnostic signals of intercalated surfactant species (*i.e.* alkyl carboxylates, mainly hydrogenated fatty acid, stearate and palmitate): strong adsorptions at 1555 cm^{-1} and 1412 cm^{-1} are indeed associated with the asymmetric and symmetric stretching modes of the carboxylate group ($RCOO^-$) and peaks at 2918 and 2850 cm^{-1} are due to asymmetric and symmetric stretching vibrations of methylene groups belonging to the organic modifier, whose fraction was about 55% wt[7,31]. However, the spectra of the composites PLA_O-LDH_1 and PLA_O-LDH_2 (Figure ESI 3) did not show significant differences in the profile of the absorp-

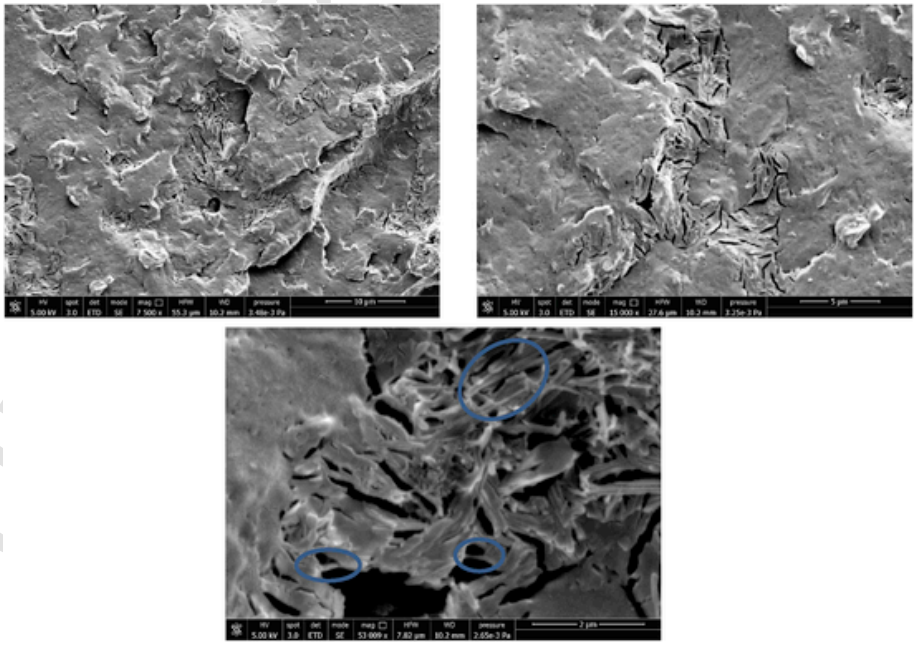

Fig. 2. SEM analysis of sample PLA_O-LDH_2 at different magnifications; the blue circles evidenced polymer fraction linking macro-aggregates and generating the flocculated structures. (For interpretation of the references to colour in this figure legend, the reader is referred to the Web version of this article.)

tion bands with respect to that of PLA, owing to the very low content of O-LDH.

The Raman spectra of O-LDH (Figure ESI 4) confirmed the presence of the organic moieties. The bands at 2883 and 2848 cm^{-1} (vs νCH_2), and other diagnostic signals at 1454 and 1434 cm^{-1} (s, δCH_2), 1295 cm^{-1} (s, $\nu C\text{-}C$), 1126 cm^{-1} (m/s, $\nu C\text{-}C$) 1096 cm^{-1} (w, $\nu C\text{-}C$) and 1059 cm^{-1} (m/s, $\nu C\text{-}C$) and 887 cm^{-1} (w, ρCH_2) are due to alkyl carboxylates, whereas the very weak peaks between 380 and 550 cm^{-1} are ascribable to vibrations of OH groups associated to Mg and Al and to stretching of Al–O–Mg; other signals can be attributed to residual carbonate and exchanged anions which are a mixture of alkyl carboxylates [33,34].

Fig. 3 reports the Raman analyses by aiming the laser on the inclusions and on the apparently free zone (polymer matrix) collected on different portions of PLA_O-LDH_2 and the spectrum of pristine PLA. The comparison revealed the presence of signals ascribable to both components. All the spectra showed the characteristic modes of PLA [35], with the main diagnostic peaks in the regions of νCH_2 and CH_3 (vs) between 3050 and 2882 cm^{-1} and at 873 cm^{-1} attributed to the $\nu C\text{-}COO$. In addition, symmetric $\nu C\text{-}CH_3$ at 1042, asymmetric νCH_3 at 1128 and asymmetric νCH groups at 1452 cm^{-1} were clearly visible and completely overlapped those of O-LDH. The spectra collected by aiming the laser over the inclusions or over an apparently free zone of the composite, showed a diagnostic signal of O-LDH (νCH_2 at 2848 cm^{-1}) not present in the pristine PLA (see Fig. 3b) suggesting a homogeneous dispersion of the nanostructured filler even if the relative peaks intensity does not reflect the sample composition, but rather the local ratio between the polymer and the O-LDH at the interface.

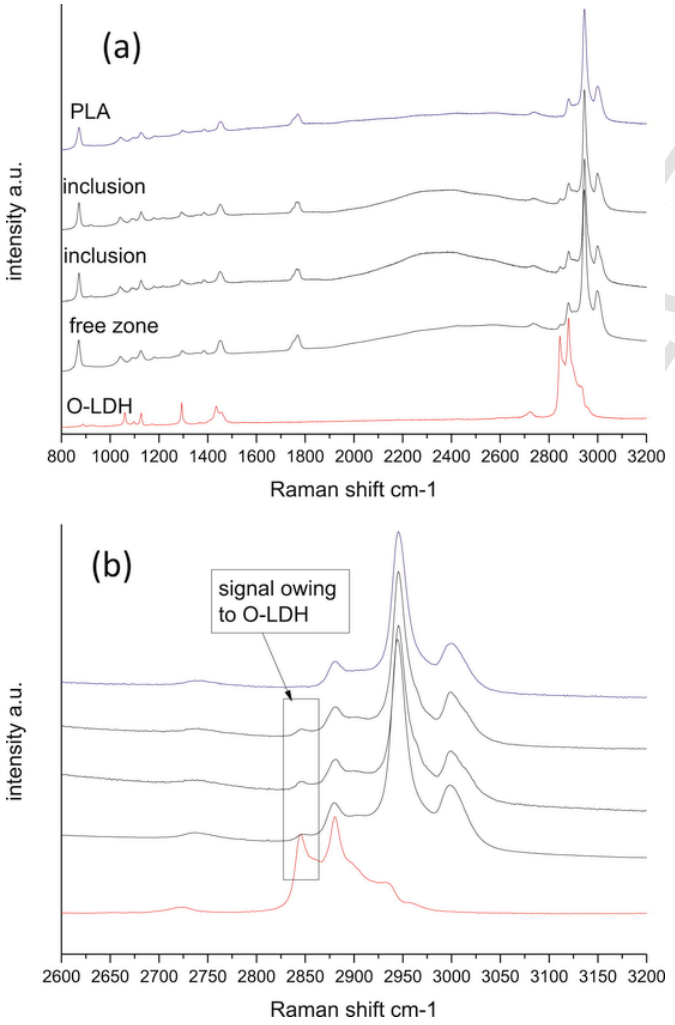

Fig. 3. (a) Raman analyses of different portions of a film of sample PLA_O-LDH_2 compared to pristine PLA (blue curve) and O-LDH (red curve); (b) enlargement of spectra in the Raman shift region of ν CH_2 and CH_3. (For interpretation of the references to colour in this figure legend, the reader is referred to the Web version of this article.)

XRD analyses were carried out onto films of all samples thermally treated at 80 °C and 130 °C in order to study the effect of different fillers onto the crystal form and size evolution of PLA in the composites during annealing procedures. Fig. 4 reports the XRD patterns of sample PLA_MgStearate annealed at 80 and 130 °C (Figure ESI 5 reports the XRD curves for all the other samples).

The comparison of the XRD patterns evidenced the shift of the intense peaks at (110)/(200) and (203/(113) and the presence of new peaks (assigned in Fig. 4) confirming, on the basis of literature, that α′- and α-crystals developed at 80 °C and 130 °C, respectively [36].

The thickness of lamellae (D) was estimated by means of the Scherrer method using the corresponding equation (eq. (2)) (i.e. *FWHM* in radians for the (203) crystallographic plan; wave-length of the radiation used $\lambda = 0.154$ nm, Bragg angle (Θ) and Scherrer constant $K = 0.95$[16,37])

$$D = (K\,\lambda)/(FWHM\,\cos\theta) \quad (2)$$

Upon increasing the annealing temperature, the crystalline domain size (D) increased, independently of sample type and composition, thus suggesting that the α-phase fostered larger crystalline domains (i.e. thermodynamically more stable phase). No significant differences were evidenced by looking at the D values for samples annealed at 130 °C, despite the different degree of crystallinity between neat PLA and composites (see Table 3), thus suggesting that the dimensions of such crystals are not affected by the presence and nature of inorganic substrate. The prolonged annealing seemed to level out any effect, even if the samples containing fewer amounts of filler (1 wt%) seem to have smaller sized crystallites. However, different contributions to line broadening of the XRD peaks, such as crystal strain and the presence of defects, due to intercalation processes has to be taken into account for these samples as more intercalated/exfoliated.

The annealing at 80 °C able to provide the crystals of α′-species resulted in D values remarkably different ranging from unfilled sample with really low mean size of the ordered (crystalline) domains with respect to filled samples having higher D values. These data suggest

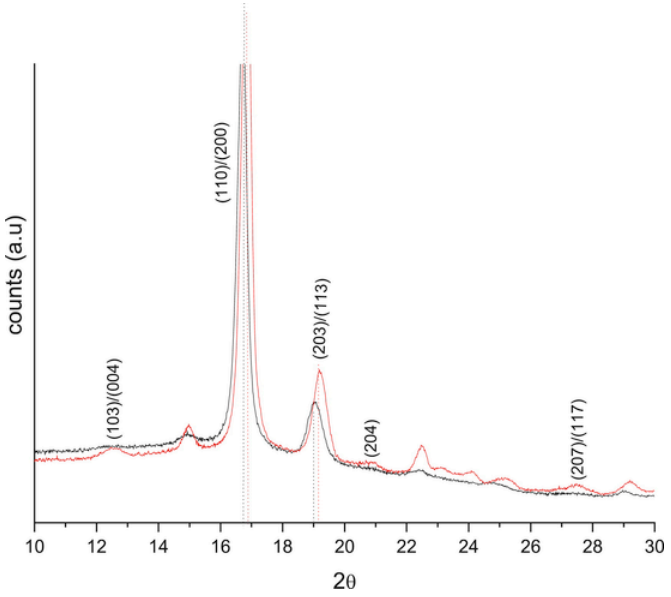

Fig. 4. XRD patterns of sample PLA_MgStearate annealed at 80 °C (black curve) and at 130 °C (red curve) for 8 h

Table 3
Thermal and structure parameters from MT-DSC.

	Quenched PLA T_{cmax} (°C)/T_{fmax} (°C)/X_c (%) [b]/X_{RAF} $_{filler}$ (%) [c]	PLA annealed at 80 °C for 8 h T_{fmax} (°C)/X_c (%) [b]/X_{RAF} (%) [c] /$X_{RAF\ crys}$ (%) [c]	PLA annealed at 130 °C for 8 h T_{cmax} (°C)/T_{fmax} (°C)/X_c (%) [b]/X_{RAF} (%) [c] /$X_{RAF\ crys}$ (%) [c]
PLA_180	100/156/0/0	155/32/18/18	99/156/39 [a]/11/11
PLA_O-LDH_1	104/156/0/4	155/32/32/28	--/156/46/18/14
PLA_O-LDH_2	105/155/0/12	154/30/38/26	--/154/45/15/3
PLA_MgStearate	100/157/0/7	156/32/24/17	--/156/48/8/1
PLA_O-LDH_1_PBSA	96/157/0/4	156/32/32/28	--/156/47/23/19

[a] $X_{c\ max}$ is not reached, there is a cold crystallization peak.
[b] Crystallinity of samples calculated from $X_c = (\Delta H_f - \Delta H_c)/\Delta H_f^0$ with $\Delta H_f^0 = 93$ J g^{-1}.
[c] Rigid amorphous fraction: $X_{RAF\ filler} = 1 - (\Delta Cp/(\omega\ \Delta Cp°))$, $X_{RAF} = 1 - (\Delta Cp/(\omega\ \Delta Cp°)) - X_c$, and $X_{RAF\ crys} = X_{RAF} - X_{RAF\ filler}$, with $\Delta Cp°$ being the heat capacity step of amorphous PLA_180 and ω the weight fraction of PLA.

the capability of all the fillers to grow the main size of crystalline domains which increased by increasing the filler dimension (PLA_O-LDH_1 vs PLA_MgStearate) and the content of O-LDH.

3.2. Thermo-mechanical properties

TGA and MT-TGA experiments of PLA and composites performed under nitrogen and oxygen atmospheres are reported in ESI 6 and Fig. 5 while the TGA of O-LDH is reported in ESI 7; they showed results globally consistent with each other although characteristic temperatures recorded from MT-TGA were lower than their equivalent from TGA. This effect may be attributed to the lower heating rate (5 °C/min *versus* 10 °C/min) and to the modulation procedure that allows obtaining a curve with better resolution. In all cases, the degradation occurs in one step.

The thermal stability of neat PLA, assessed by standard TGA was weakly dependent on the atmosphere used to carry out the analysis. Thermo-oxidative degradation of PLA in the solid state occurs by random chain scission reactions after the formation of peroxy radicals and hydroperoxides but similar weight loss curves *versus* temperature are generally reported in literature also in the case of inert atmosphere: the decomposition pattern of neat PLA in oxygen is similar to that in the inert atmosphere [38–41]. Interestingly, MT-TGA helps evidencing a stabilizing effect of oxygen since the degradation temperature of PLA recorded under oxygen atmosphere shifted to significantly higher values than that recorded under nitrogen. This stabilizing effect of oxygen has been discussed for other polymers. Peterson et al. [42,43] have reported that the presence of oxygen (their study was performed under air atmosphere) increases the initial decomposition temperature of poly (methyl methacrylate) by 70 °C. They assumed that this behaviour results from competitive reactions leading to the formation of thermally stable radical species that suppress the unzipping of polymer. The competition between different reactions under oxygen atmosphere was also investigated by Wang et al. [44] in polyacrylonitrile fibers. One may consider that the hydroperoxides formation and decomposition may delay the chain breaking events. The discrepancy between TGA and MT-TGA data may result from different diffusion capability of oxygen in the sample analysed by MT-TGA owing to reduced heating rate typical of this experimental condition, with respect to TGA experiments. This can enhance the effects related to possible reaction between polymer and oxygen.

Regarding the nanocomposites, the shift to higher degradation temperatures under oxygen atmosphere was recorded from both techniques, suggesting that the stabilizing effect of oxygen is even more pronounced with the addition of fillers. The mechanism behind is not straightforward however. The observed shift is very pronounced for PLA_O-LDH_1 and PLA_MgStearate (i.e. both latter composites exhibited the lowest amount of filler among those studied herein).

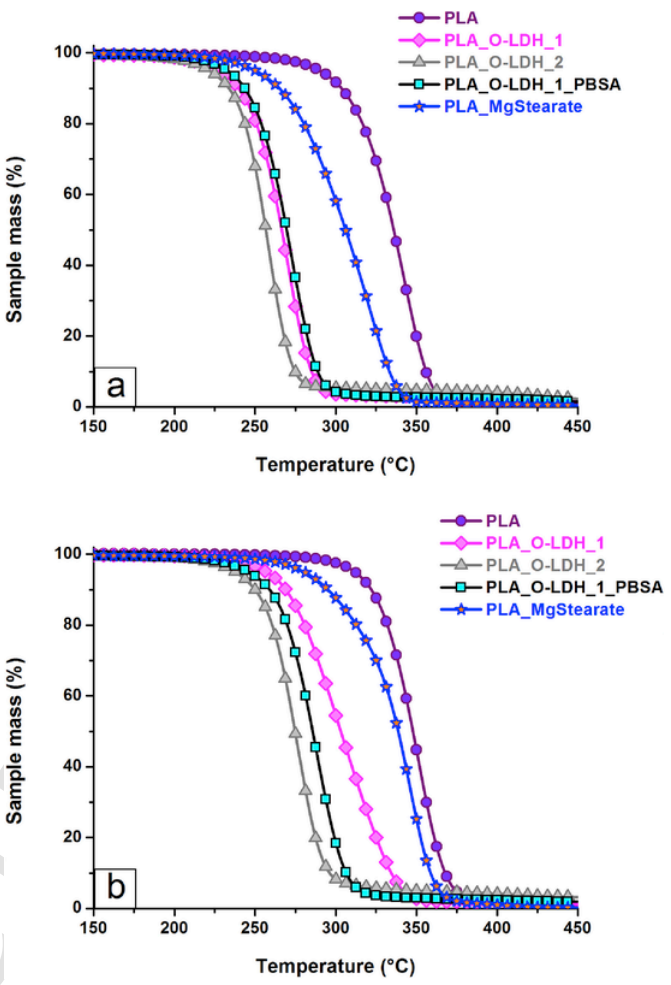

Fig. 5. MT-TGA curves of PLA and composite samples acquired under (a) nitrogen and (b) oxygen atmosphere.

The presence of nanofillers favored the thermal degradation process, regardless of the nature of the atmosphere used (results shown in Table ESI 1) [12,17,22,28]. One may attribute this result to the interfaces between the matrix and the filler that create additional preferential area for initiating and propagating the degradation. As already reported in the literature [30], the TGA analysis carried out onto O-LDH (Figure ESI 7) shows different steps and in particular the loss of adsorbed water, the loss of adsorbed anions which degrade at around 290–320 °C and then the degradation of the intercalated anions together with the dehydroxylation of the inorganic layers (between 250 and 450 °C). These degradative steps and the associated reaction products, especially water molecules, $Mg(OH)_2$ and MgO resulting from dehydroxylation reaction, can affect the thermal stability of intercalated PLA chains causing the random breaking of polymer chains and producing oligomers and lactide at lower temperatures with respect to unfilled polymer by unzipping depolymerisation mechanism [12,17,22,28]. As shown in Fig. 5 and in Table ESI 1, these effects were more pronounced when the filler weight percentage increased and by using the polymer coupling agent PBSA which is probably able to intercalate the piled O-LDH layers [45] favoring the interfacial interaction between the filler and the polymer matrix. The lowest degrada-

tion temperature values are, indeed, obtained for PLA_O-LDH_2 and PLA_O-LDH_1_PBSA.

The addition of the macrofiller (MgStearate) has not the same effect. In PLA_MgStearate the mass loss occurred for higher temperatures in comparison with PLA_O-LDH_1. The higher thermal stability of PLA_MgStearate with respect to PLA_O-LDH_1 confirmed that the degradation is mainly activated by the inorganic component of hybrid (the layered hydroxides) whose interaction with polymer chains is more effective when modified with carboxylate (as surfactant). At the same time, the smaller interfacial surfaces characteristic of microcomposite (PLA_MgStearate) in comparison with nanocomposite (PLA_O-LDH_1) reduces the possibility or the extent of any degradation reactions activated by carboxylate, even if the latter have a certain effectiveness with respect to pristine PLA [46].

The activation energy (E_a) calculated from MT-TGA measurements (Fig. 6 and experimental part for details) was consistent with these observations, and for the analysis carried out under nitrogen the E_a trend with respect to mass loss partially reflects that previously discussed [17]. Interestingly, in our testing experiments, E_a in the middle stage of degradation was higher under oxygen than under nitrogen, for all

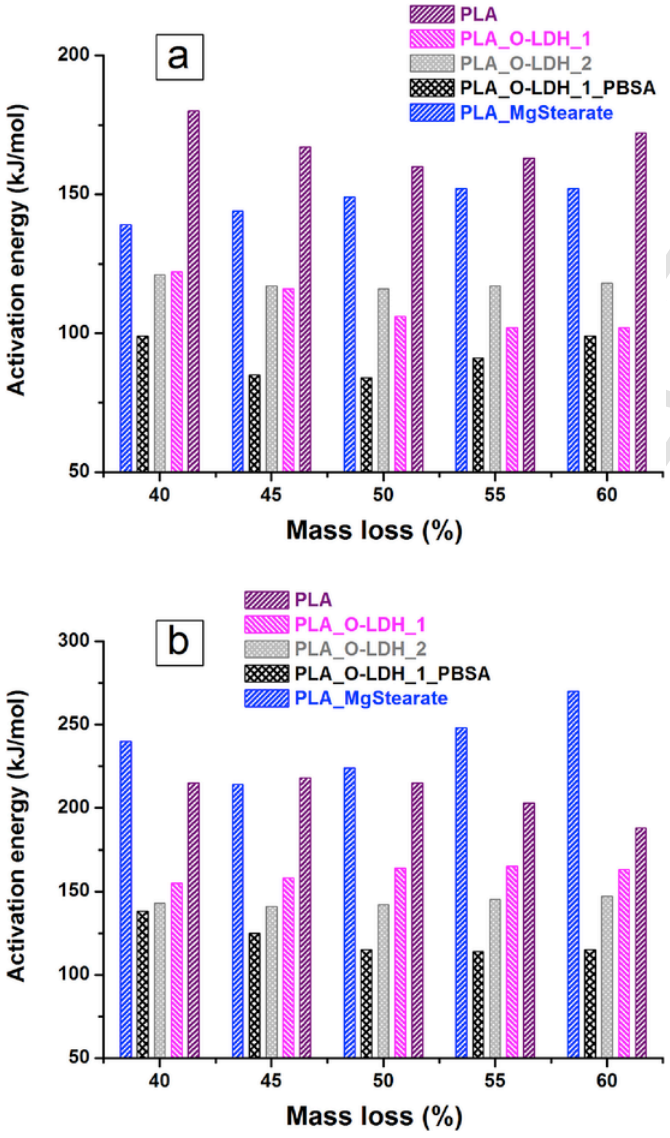

Fig. 6. Activation Energy evaluated from MT-TGA curves under (a) nitrogen and (b) oxygen atmosphere.

the systems, suggesting the formation of stable species during thermo oxidative degradation of both neat PLA and PLA_O-LDH nanocomposites. This behaviour, although not discussed in depth, was reported by Babanalbandi et al. [47] conducting conventional TGA. It is also remarkable that the activation energy for PLA_MgStearate was slightly lower under nitrogen, but higher when the experiment was performed under oxygen, compared to neat PLA, whereas the introduction of O-LDH led to a strong decrease of activation energy under both oxygen and nitrogen atmosphere. This definitely confirmed the impact of the filler's nature on the thermal stability and proved that the presence of O-LDH contributes to accelerate degradation.

The main thermal transition values of samples were determined from DSC investigations. Fig. 7 shows the calorimetric signatures for quenched and annealed samples. Table 3 gives the values of all the parameters extracted from these curves.

Quenched samples (Fig. 7a) exhibited the classical behaviour of PLA (i.e. an endothermic step around 55 °C corresponding to the glass transition, a cold crystallization around 100 °C leading to the concomitant crystallization under both α- and α′-forms, and finally a complex melting double peak around 150 °C, as widely reported in literature [36,48]). Interestingly, PLA showed a better ability to cold crystallize in the presence of MgStearate (1% w/w) compared to neat PLA. On the contrary, a sort of delay in cold crystallization of samples containing O-LDH can be observed with respect to PLA_MgStearate, which is presumably due to smaller size of dispersed particles and to larger surface of polymer-filler interaction.

Samples annealed at 80 °C (Fig. 7b) showed the endothermic step at the glass transition lower than in the case of the rejuvenated sample (in agreement to the presence of crystalline phase). At higher temperature an exothermic peak corresponding to the reorganization of the α′-crystalline form to α-one [49] and an endothermic peak related to the melting of α-form appeared whatever the sample. The samples annealed at 130 °C (Fig. 7c) showed similar low endothermic steps at the glass transition than those annealed at 80 °C, but only an endothermic peak at higher temperature (about 155 °C) and related to the melting of α form as expected [50]. For all thermal treatments, the melting temperatures coincide among samples with an uncertainty of ±1 °C.

Furthermore, among the samples annealed at 130 °C, only in the case of neat PLA, an exothermic peak around 100 °C due to the cold crystallization was observed. The presence of this peak unequivocally demonstrates the role of the fillers as nucleating agents and their ability to induce the crystallization of the polymer. This evidence was also confirmed by the degree of crystallinity X_c, reported in Table 3, which is higher in composites than in neat PLA, assessing the nucleation effects of the filler despite its nature and shape. While the formation of the more ordered α-form growing at 130 °C is speeded-up by the presence of micro-and nanofiller, it is not possible to ascertain a nucleation effect at 80 °C with all samples having reached their maximum degree of crystallinity. Moreover, the cold-crystallization temperatures of quenched amorphous samples (Fig. 7a) did not evidence a clear trend among samples. It might indicate a more complex morphological dependence of the nucleation mechanism with temperature.

By comparing the heat capacity step of any sample in comparison to amorphous PLA_180, it is possible to determine the content of amorphous phase which mobility is restricted, either by the nanofillers or by the crystals. This corresponds to the rigid amorphous fraction (X_{RAF}) that does not contribute to the heat capacity increment associated with the glass transition. In amorphous samples, RAF forms around the fillers ($X_{RAF\ filler}$) [50–53], whereas in semi-crystalline samples it also forms in the vicinity of the crystals ($X_{RAF\ crys}$) when macromolecules difficultly rearrange into crystals. It is assumed that $X_{RAF\ filler}$ is independent on the thermal history. Therefore $X_{RAF\ crys}$ is simply deduced by subtracting $X_{RAF\ filler}$ from X_{RAF} (Table 3).

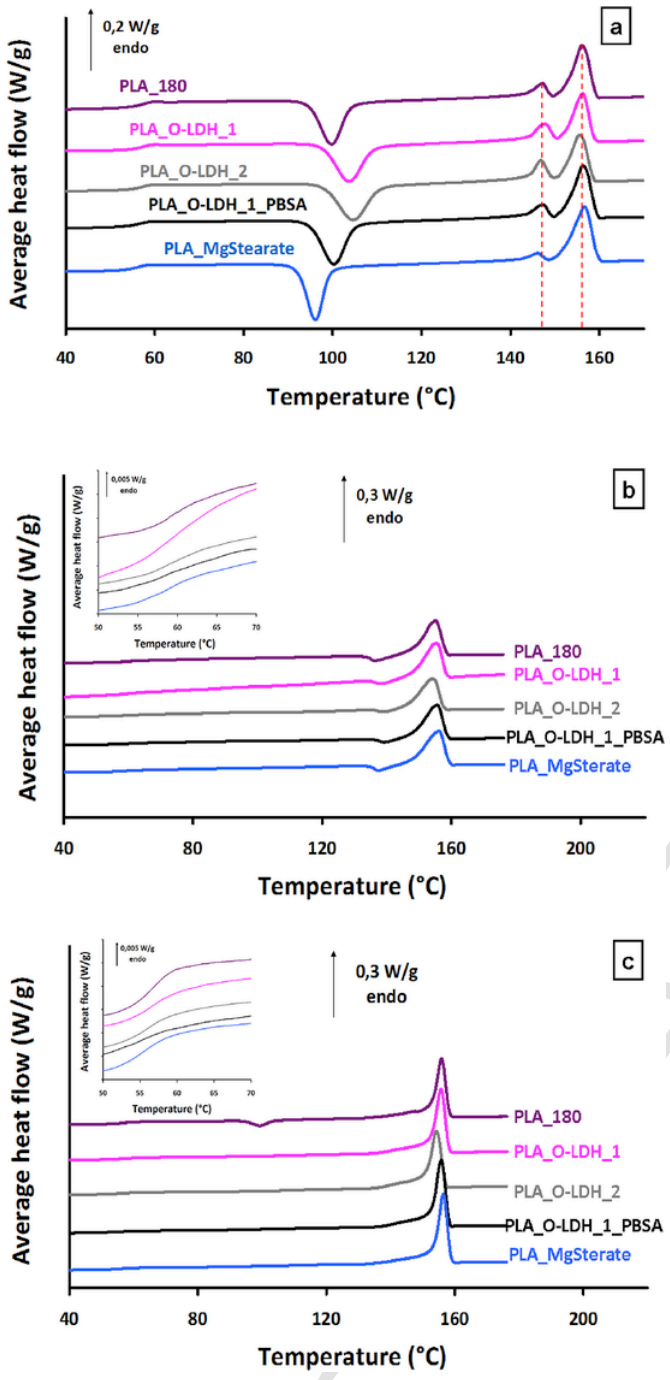

Fig. 7. Evolution of the normalized average heat flow as a function of temperature for all the samples after quenching (a) and annealing at 80 °C (b) and 130 °C (c) respectively for 8 h. Insets are showing the glass transition domain for semi-crystalline samples. In all figures, the curves are shifted for clarity.

$X_{RAF\ filler}$ increases with the content of O-LDH, reaching values up to 12% for PLA_O-LDH_2 whereas it does not differ between PLA_O-LDH_1 and PLA_O-LDH_1_PBSA. Interestingly, these results correlate with thermogravimetric analyses which show a poor thermal stability for samples containing O-LDH, and the worst for PLA_O-LDH_2. Since RAF in PLA is generally reported as a less dense part of the amorphous phase [54] located close at the filler surface, one may assume that it constitutes a privileged path for reactive species formed at interface. In fact several authors reported that $X_{RAF\ crys}$ increases with the decrease of the annealing temperature [55,56]. By crystallizing at 80 °C, $X_{RAF\ crys}$ is higher in samples containing O-LDH than in neat PLA, suggesting that O-LDH hinders the crystal packing. However at 130 °C, the addition of O-LDH shows no, or opposite, effect. It has previously been shown by Leng et al. [53] that there is no linear relation between $X_{RAF\ filler}$ and $X_{RAF\ crys}$. We observe, moreover, that $X_{RAF\ crys}$ could be either promoted or inhibited depending on the crystallization conditions.

In PLA_MgStearate $X_{RAF\ filler}$ = 7%, but RAF has less incidence on thermal stability than other fillers for the reasons given in the discussion of thermogravimetric measurements. Moreover, in this system, $X_{RAF\ crys}$ is globally low in comparison to nanocomposites. Although one could tentatively relate $X_{RAF\ crys}$ to the interfacial area, knowing that the surface/volume ratio increases opposite to the size of the filler, further investigations are needed to explain this results.

The effects of annealing on the mechanical properties of PLA and PLA composites were even investigated and results are reported in Table 4. Young Modulus (*E*) tensile strength (*TS*) and elongation at break (*EB*) of samples after annealing at 80 °C are compared with those of quenched samples.

Before annealing, all the composites showed increased values of the modulus with respect to PLA_180 sample in agreement with the reinforcing effect exerted by dispersed filler.

TS is higher for PLA_MgStearate in comparison to that of PLA_180, but *EB* was similar, suggesting that the addition of microfiller even in low/modest quantity increases the plastic response, especially with reference to Young Modulus and mechanical resistance to applied load (*TS*).

The samples containing the nanofiller (O-LDH) were characterized by lower values of *TS* and *EB* compared to PLA_180, in agreement with data reported in literature [57]; in addition, by increasing the amount of O-LDH a negative trend can be observed and the composite PLA_O-LDH_2 appears more brittle with respect to the matrix and to the other composites. This result can be tentatively correlated to the amount of interfaces among nanocomposites, i.e., $X_{RAF\ filler}$, which is the higher for that sample and can negatively affect the plastic deformation capability of the specimen.

After annealing at 80 °C the microcomposite (PLA_MgStearate) showed a behaviour completely comparable to that of PLA_180, which improved the mechanical performances with reference to *E* and *TS* by keeping unchanged the elongation, whereas, nanocomposites showed lower values for *TS* and the *EB*, despite the increase of the modulus. Once again the sample containing higher quantity of O-LDH showed higher detriment of *TS* and *EB* values. This trend, already reported for similar nanocomposites subjected to reprocessing [57], is probably ascribable to different phenomena. First of all there is an increase of crystallinity that could raise the stiffness as evidenced by the increase of *E*, shown for all the samples by comparing the data before and after annealing. All the samples are characterized by similar crystallinity, but samples containing O-LDH strengthen and stiffen by developing a substantially higher $X_{RAF\ crys}$. In addition, during annealing, even if carried out in static condition, further intercalation processes of polymer chains into the O-LDH layers can enlarge the fraction of the exfoliated material and thus of polymer chains which, as accommodated in proximity of (or between) the layers, are characterized by reduced mobility, likely increasing the whole material stiffness and its brittleness. This can partially justify the ductility loss evidenced especially for samples having better dispersion, which means in the presence of coupling agent (PBSA), and/or higher content of O-LDH. However, together with increased crystallinity and nanofiller dispersion, different effects like as a certain molecular weight reduction [13,57], owing to prolonged annealing and possibly affecting the mechanical performances of PLA [58], cannot be completely excluded.

Table 4
Mechanical properties of PLA and its composites.

Sample Property [a]	PLA_180	PLA_O-LDH_1	PLA_O-LDH_2	PLA_O-LDH_1_PBSA	PLA_MgStearate
E (MPa)	5000 ± 450	5200 ± 300	5090 ± 150	5300 ± 250	5500 ± 100
TS (MPa)	46.0 ± 3.0	44.9 ± 1.5	30.5 ± 3.2	40.6 ± 0.5	56.8 ± 1.0
EB %	1.3 ± 0.09	1.2 ± 0.05	0.69 ± 0.06	1.0 ± 0.05	1.4 ± 0.07
E (MPa)$_{80}$	5400 ± 500	5600 ± 350	5400 ± 150	5900 ± 300	5400 ± 240
TS (MPa)$_{80}$	52.4 ± 3.4	43.9 ± 1.8	21.5 ± 5.6	36.8 ± 2.1	52.4 ± 1.6
EB %$_{80}$	1.3 ± 0.23	1.0 ± 0.12	0.46 ± 0.11	0.7 ± 0.03	1.1 ± 0.12

[a] Performed onto 5 replicates and averages calculated by eliminating the extreme values.

4. Conclusions

Composites of PLA with organo-modified LDH were prepared by melt blending process and characterized with respect to morphology and thermomechanical features. The characteristic diffraction peaks of O-LDH were not visible in XRD patterns of PLA/O-LDH samples thus suggesting an exfoliated morphology, but disordered microaggregates possibly formed by flocculation were evidenced by SEM. This effect was more evident by increasing the content of O-LDH. Interestingly, the micro Raman analysis of microaggregates/inclusions revealed that they are composed by both PLA and O-LDH phases and are characterized by a good interaction between polymer chains and inorganic layers not in parallel registry. A certain decrement of PLA molecular weight was observed by increasing the O-LDH content or enlarging the interfacial surface.

The thermal stability of the composites depended on the nature and content of filler; generally a decrease of thermal stability is evidenced by adding the filler. All the composites showed a reduction in the values of the activation energy in the middle stage of degradation ranging from 40 to 60%, but microsized filler (MgStearate) and/or low content of O-LDH retained the degradation effects particularly in the oxygen atmosphere. In general all the factors/parameters improving the interactions between the polymer chains and the inorganic substrates such as the increase of the content of nanofiller or the use of a coupling agent decreased the thermal stability, definitely assessing that the chemical nature of LDH, that means the magnesium aluminium hydroxides, induced an acceleration of degradation reactions of PLA. Fewer effects were observed for the sample PLA_MgStearate proving that the carboxylates used as surfactants did not provoke extensive degradation of PLA.

Even crystallinity, content of RAF, and size of crystalline domains are affected by nature and content of filler upon the different annealing processes. To summarize the salient results regarding the different behaviour of filled and un-filled samples (with micro- and nano-filler), the main findings related to the structure/properties as a function of the annealing temperature are following reported.

Finding	Samples annealed at 80 °C	Samples annealed at 130 °C
Crystals form	α′	α
Nucleation	Not evidenced	Promoted by the filler (micro and nano)
RAF	About 20–40% increased by nanofiller	About 10–20% weakly increased with filler content in nanocomposites and not increased in microcomposite
X_{RAF} $_{crys}$	promoted by adding nanofiller	not promoted by adding filler, sometimes even inhibited
Crystallite size (D)	greatly enhanced with the addition of filler	in the same order, sometimes slightly smaller with the addition of filler

By annealing the samples at 80 °C, which induced a predominant formation of α' crystalline (metastable) phase, the size of crystalline domains and the RAF content were both higher for the nanocomposites in comparison to unfilled PLA. These results suggested that in this condition the filler partially hinders the decoupling between crystal and amorphous, but not the crystal growth.

In contrast, by annealing the samples at 130 °C (generating a predominant content of α crystalline phase), the size of crystalline domains is in the same order among samples. The RAF content is less in comparison to the annealing at 80 °C, as expected. However, RAF associated to crystallization is not promoted by the filler addition. Even more surprising, its content is only significant in samples where the dispersion and thus the interfacial interactions are more effective (the sample with lower content of O-LDH and prepared with the coupling agent). From the collected data we evidenced a complex dependence of the microstructure on the crystallization conditions through opposite structural effects regarding the size of the crystals and the RAF behaviour.

Finally the mechanical features of the nanocomposites showed higher modulus by filler dispersion and owing to annealing at 80 °C; moreover, the experimental data suggested a certain increase of the stiffness and a general loss of ductility with respect to un-filled polymer likely due to further improvements of nanofiller dispersion.

CRediT authorship contribution statement

Nicolas Delpouve: Conceptualization, Methodology, Data curation, Investigation, Writing - original draft. **Allisson Saiter-Fourcin:** Conceptualization, Methodology, Data curation, Investigation, Writing - review & editing, Supervision. **Serena Coiai:** Conceptualization, Writing - review & editing, Investigation, Resources. **Francesca Cicogna:** Conceptualization, Writing - review & editing, Investigation. **Roberto Spiniello:** Investigation. **Werner Oberhauser:** Investigation, Data curation, Writing - review & editing. **Stefano Legnaioli:** Investigation, Data curation, Writing - review & editing. **Randa Ishak:** Investigation. **Elisa Passaglia:** Conceptualization, Methodology, Data curation, Writing - original draft, Writing - review & editing, Visualization, Supervision, Project administration.

CRediT authorship contribution statement

Nicolas Delpouve: Conceptualization, Methodology, Data curation, Investigation, Writing - original draft. **Allisson Saiter-Fourcin:** Conceptualization, Methodology, Data curation, Investigation, Writing - review & editing, Supervision. **Serena Coiai:** Conceptualization, Writing - review & editing, Investigation, Resources. **Francesca Cicogna:** Conceptualization, Writing - review & editing, Investigation. **Roberto Spiniello:** Investigation. **Werner Oberhauser:** Investigation, Data curation, Writing - review & editing. **Stefano Legnaioli:** Investigation, Data curation, Writing - review & editing. **Randa Ishak:** Investigation. **Elisa Passaglia:** Conceptualization, Methodology, Data cura-

tion, Writing - original draft, Writing - review & editing, Visualization, Supervision, Project administration.

Declaration of competing interest

The authors declare that they have no known competing financial interests or personal relationships that could have appeared to influence the work reported in this paper.

Acknowledgements

MIUR (PRIN 2008) Contract grant number: 200898KCKY is acknowledged for partially funding the research.

Appendix A. Supplementary data

Supplementary data to this article can be found online at https://doi.org/10.1016/j.polymer.2020.122952.

Uncited references

[32], [37].

References

[1] J-W Rhim, H-M Park, C-S Ha, Bio-nanocomposites for food packaging applications, Prog. Polym. Sci. 38 (2013) 1629–1652.
[2] M E Drieskens, R Peeters, J Mullens, D Franco, P J Lemstra, D G Hristova-Bogaerds, Structure versus properties relationship of poly(lactic acid). I. Effect of crystallinity on barrier properties, J. Polym. Sci., Part B: Polym. Phys. 47 (2009) 2247–2258.
[3] S Fernandes Nassar, A Guinault, N Delpouve, V Divry, V Ducruet, C Sollogoub, S Domenek, Multi-scale analysis of the impact of polylactide morphology on gas barrier properties, Polymer 108 (2017) 163–172.
[4] Z D Demirkay, B Sengul, M S Eroglu, N Dilsiz, Comprehensive characterization of polylactide-layered double hydroxides nanocomposites as packaging materials, J. Polym. Res. 22 (2015) 124.
[5] Z Geng, W Zhen, Z Song, X Wang, Structure and performance of poly (lactic acid)/amide ethylenediamine tetraacetic acid disodium salt intercalation layered double hydroxides nanocomposites, J. Polym. Res. 25 (2018) 115.
[6] X Bi, H Zhang, L Dou, Layered double hydroxide-based nanocarriers forDrug delivery, Pharmaceutics 6 (2014) 298–332.
[7] S Coiai, L Pérez Amaro, F Cicogna, N Tz Dintcheva, F Liguori, P Barbaro, E Passaglia, Progress towards the understanding of the interactions between functionalized polyolefins and organo-layered double hydroxides, Macromol. React. Eng. 8 (2014) 122–133.
[8] R Arrigo, N Tzankova Dintcheva, G Tarantino, E Passaglia, S Coiai, F Cicogna, S Filippi, G Nasillo, D Chillura Martino, An insight into the interaction between functionalized thermoplastic elastomer and layered double hydroxides through rheological investigations, Compos. B Eng. 139 (2018) 47–54.
[9] S Coiai, F Cicogna, A de Santi, L Pérez Amaro, R Spiniello, F Signori, S Fiori, W Oberhauser, E Passaglia, MMT and LDH organo-modification with surfactants tailored for PLA nanocomposites, Express Polym. Lett. 11 (2017) 163–175.
[10] R Scaffaro, L Botta, E Passaglia, W Oberhauser, M Frediani, L Di Landro, Comparison of different processing methods to prepare poly(lactic acid)-hydrotalcite composites, Polym. Eng. Sci. 54 (2014) 1804–1810.
[11] N Gerds, V Katiyar, C Bender Koch, H C B Hansen, D Plackett, E H Larsen, J Risbo, Degradation of l-polylactide during melt processing with layered double hydroxides, Polym. Degrad. Stabil. 97 (2012) 2002–2009.
[12] V Katiyar, N Gerds, C Bender Koch, J Risbo, H C B Hansen, D Plackett, Melt processing of poly(L-lactic acid) in the presence of organomodified anionic or cationic clays, J. Appl. Polym. Sci. 122 (2011) 112–125.
[13] L Pérez Amaro, F Cicogna, E Passaglia, E Morici, W Oberhauser, S Al-Malaika, N Tzankova Dintcheva, S Coiai, Thermo-oxidative stabilization of poly(lactic acid) with antioxidant intercalated layered double hydroxides, Polym. Degrad. Stabil. 133 (2016) 92–100.
[14] S Coiai, S Javarone, F Cicogna, W Oberhauser, M Onor, A Pucci, P Minei, G Iasilli, E Passaglia, Fluorescent LDPE and PLA nanocomposites containing fluorescein-modified layered double hydroxides and their ON/OFF responsive behavior towards humidity, Eur. Polym. J. 99 (2018) 189–201.
[15] N Muksing, R Magaraphan, S Coiai, E Passaglia, Effect of surfactant alkyl chain length on the dispersion, and thermal and dynamic mechanical properties of LDPE/organo-LDH composites, Express Polym. Lett. 5 (2011) 428–448.
[16] J Leng, N Kang, D-Y Wang, J Falkenhagen, A F Thünemann, A Schönhals, Structure–Property relationships of nanocomposites based on polylactide and layered double hydroxides–comparison of MgAl and NiAl LDH as nanofiller, Macromol. Chem. Phys. 218 (2017) 1700232.
[17] M F Chiang, M-Z Chu, T-M Wu, Effect of layered double hydroxides on the thermal degradation behavior of biodegradable poly(L-lactide) nanocomposites, Polym. Degrad. Stabil. 96 (2011) 60–66.
[18] P Ding, B Kang, J Zhang, J Yang, N Song, S Tang, L Shi, Phosphorus-containing flame retardant modified layered double hydroxides and their applications on polylactide film with good transparency, J. Colloid Interface Sci. 440 (46–52) (2015).
[19] A Oyarzabal, A Mugica, A J Mueller, M Zubitur, Hydrolytic degradation of nanocomposites based on poly(lactic acid) and layered double hydroxides modified with a model drug, J. Appl. Polym. Sci. 43648 (2016).
[20] J Leng, P J Purohita, N Kang, D-Y Wang, J Falkenhagen, F Emmerling, A F Thünemann, A Schönhals, Structure–property relationships of nanocomposites based on polylactide and MgAl layered double hydroxides, Eur. Polym. J. 68 (2015) 338–354.
[21] M Monshizadeh, S Seifi, I Hejazi, J Seyfi, H Ali Khonakdar, Enhanced properties of poly(lactic acid) by concurrent addition of organo-modified Mg-Al layered double hydroxide (LDH) and triethyl citrate, J. Thermoplast. Compos. Mater. 1–16 (2019).
[22] T Nogueira, N Gonçalves, R Botan, F Wypych, L Lona, Layered double hydroxides as fillers in poly(l-lactide) nanocomposites, obtained by in situ bulk polymerization, Polímeros 26 (2) (2016) 106–114.
[23] R L Blaine, B K Hahn, Obtaining kinetic parameters by modulated thermogravimetry, J. Therm. Anal. 54 (1998) 695–704.
[24] V Mamleev, S Bourbigot, Modulated thermogravimetry in analysis of decomposition kinetics, Chem. Eng. Sci. 60 (2005) 747–766.
[25] R R Keuleers, J F Janssens, H O Desseyn, Comparison of some methods for activation energy determination of thermal decomposition reactions by thermogravimetry, Thermochim. Acta 385 (2002) 127–142.
[26] J E K Schawe, A general approach for temperature modulated thermogravimetry: extension to non-periodical and event-controlled modulation, Thermochim. Acta 593 (2014) 65–70.
[27] C A Gracia-Fernandez, S Gomez-Barreiro, S Ruız-Salvador, R Blaine, Study of the degradation of a thermoset system using TGA and modulated TGA, Progr. Org. Coat. 54 (2005) 332–336.
[28] T Motoyama, T Tsukegi, Y Shirai, H Nishida, T Endo, Effects of MgO catalyst on depolymerization of poly-L-lactic acid to L,L-lactide, Polym. Degr. Stab. 92 (2007) 1350–1358.
[29] M Eili, K Shameli, N A Ibrahim, W M Z Wan Yunus, Degradability enhancement of poly (lactic acid) by stearate-Zn3Al LDH nanolayers, Int. J. Mol. Sci. 13 (2012) 7938–7951.
[30] S Coiai, M Scatto, L Conzatti, F Azzurri, L Andreotti, E Salmini, P Stagnaro, Al Zanolin, F Cicogna, E Passaglia, Optimization of organo-layered double hydroxide dispersion in LDPE-based nanocomposites, Polym. Adv. Techn. 22 (2011) 2285–2294.
[31] S Coiai, E Passaglia, A Hermann, S Augier, D Pratelli, R C Streller, The influence of the compatibilizer on the morphology and thermal properties of polypropylene layered double hydroxide composites" Polym, Compos 31 (2010) 744–754.
[32] V Otero, D Sanches, C Montagner, M Vilarigues, L Carlyle, J A Lopes, M J Melo, Characterization of metal carboxylates by Raman and infrared spectroscopy in works of art, J. Raman Spectrosc. 45 (2014) 1197–1206.
[33] P Du, S Qiu, C Liu, G Liu, H Zhao, L Wang, In situ polymerization of sulfonated polyaniline in layered double hydroxide host matrix for corrosion protection, New J. Chem. 42 (2018) 4201–4209.
[34] L P F Benício, D Eulálio, L de Moura Guimarães, F Garcia Pinto, L Marciano da Costa, J. Tronto "Layered double hydroxides as hosting matrices for storage and slow release of phosphate analyzed by stirred-flow method" Mat, Res. 21 (6) (2018) e20171004.
[35] P B Smith, A Leugers, S Kang, X Yang, S L Hsu, Raman Characterization of orientation in poly(lactic) acid films, Macromol. Symp. 175 (2001) 81–94.
[36] M C Righetti, M Gazzano, M L Di Lorenzo, R Androsch, Enthalpy of melting of α'- and α-crystals of pol(l-lactic acid), Eur. Polym. J. 70 (2015) 215–220.
[37] T Farid, V N Herrera, O Krístina, Investigation of crystalline structure of plasticized poly(lactic acid) banana nanofibers composites, IOP Conf. Ser. Mater. Sci. Eng. 369 (2018) 012031.
[38] K Berger, A Gregorova, Thermal stability of modified end-capped poly(lactic acid), J. Appl. Polym. Sci. 131 (2014) 41105.
[39] R Arrigo, E Morici, N Tz Dintcheva, Biopolyester-based systems containing naturally occurring compounds with enhanced thermo-oxidative stability, J. Appl. Biomater. Funct. Mater. 14 (2016) e455–e462.
[40] D Rasselet, A Ruellan, A Guinault, G Miquelard-Garnier, C Sollogoub, B Fayolle, Oxidative degradation of polylactide (PLA) and its effects on physical and mechanical properties, Eur. Polym. J. 50 (2014) 109–116.
[41] S Lv, Y Zhang, H Tan, Thermal and thermo-oxidative degradation kinetics and characteristics of poly(lactic acid) and its composites, Waste Manag. 87 (2019) 335–344.
[42] J D Peterson, S Vyazovkin, C A Wight, Kinetic study of stabilizing effect of oxygen on thermal degradation of poly(methylmethacrylate), J. Phys. Chem. B 103 (1999) 8087–8092.
[43] J D Peterson, S Vyazovkin, C A Wight, Stabilizing effect of oxygen on thermal degradation of poly(methyl methacrylate" Macromol, Rapid Commun 20 (1999) 480–483.
[44] J Wang, Lg Hu, C Yang, W Zhao, Y Lu, Effects of oxygen content in the atmosphere on thermal oxidative stabilization of polyacrylonitrile fibers, RSC Adv. 6 (2016) 73404–73411.
[45] T Malwela, S Sinha Ray, Role of organoclay in controlling the morphology and crystal-growth behaviour of biodegradable polymer-blend thin films studied using Atomic Force Microscopy, Macromol. Mater. Eng. 299 (2014) 1106–1115.
[46] Y Fan, H Nishida, S Hoshihara, Y Shirai, Y Tokiwa, T Endo, Pyrolysis kinetics of poly(l-lactide) with carboxyl and calcium salt end structures, Polym. Degrad. .Stab. 79 (2003) 547–562.
[47] A Babanalbandi, D J T Hill, D S Hunter, L Ketlle, Thermal stability of poly(lactic acid) before and after γ-radiolysis, Polym. Int. 48 (1999) 980–984.

[48] N Delpouve, A Saiter, E Dargent, Cooperativity length evolution during crystallization of poly(lactic acid), Eur. Polym. J. 47 (2011) 2414–2423.
[49] J Zhang, K Tashiro, H Tsuji, A J Domb, Disorder-to-order phase transition and multiple melting behavior of poly (l-lactide) investigated by simultaneous measurements of WAXD and DSC, Macromolecules 41 (2008) 1352–1357.
[50] A Saiter, N Delpouve, E Dargent, W Oberhauser, L Conzatti, F Cicogna, E Passaglia, Probing the chain segment mobility at the interface of semi-crystalline polylactide/clay nanocomposites, Eur. Polym. J. 78 (2016) 274–289.
[51] A Sargsyan, A Tonoyan, S Davtyan, C Schick, The amount of immobilized polymer in PMMA SiO2 nanocomposites determined from calorimetric data, Eur. Polym. J. 43 (2007) 3113–3127.
[52] A Wurm, M Ismail, B Kretzschmar, D Pospiech, C Schick, Restarted crystallization in polyamide/layered silicates nanocomposites caused by an immobilized interphase, Macromolecules 43 (2010) 1480–1487.
[53] J Leng, P Szymoniak, N-J Kang, D-Y Wang, A.s Wurm, C. Schick, A. Schönhals "Influence of interfaces on the crystallization behavior and the rigid amorphous phase of poly(l-lactide)-based nanocomposites with different layered doubled hydroxides as nanofiller, Polymer 184 (2019) 121929.
[54] J del Rio, A Etxeberria, N Lopez–Rodriguez, E Lizundia, J–R Sarasua, A PALS contribution to the supramolecular structure of poly(l–lactide), Macromolecules 43 (2010) 4698–4707.
[55] M C Righetti, E Tombari, Crystalline, mobile amorphous and rigid amorphous fractions in poly(L-lactic acid) by TMDSC, Thermochim. Acta 522 (2011) 118–127.
[56] N Varol, N Delpouve, S Araujo, S Domenek, A Guinault, R Golovchak, A Ingram, L Delbreilh, E Dargent, Amorphous rigidification and cooperativity drop in semi−crystalline plasticized polylactide, Polymer 194 (2020) 122373.
[57] R Scaffaro, F Sutera, M C Mistretta, L Botta, F P La Mantia, Structure-properties relationships in melt reprocessed PLA/hydrotalcites nanocomposites, Express Polym. Lett. 7 (2017) 555–564.
[58] G Perego, G D Cella, C Bastioli, Effect of molecular weight and crystallinity on poly(lactic acid) mechanical properties, J. Appl. Polym. Sci. 59 (1996) 37–43.